

This Prospectus for a Dissertation
entitled
PLASMA FLOW CONTROL
FOR NOISE REDUCTION
ON A G550 NOSE LANDING GEAR: THE DEVELOPMENT OF A PLASMA
FAIRING

typeset with `NDDiss2 ε` v3.2013 (2013/04/16) on December 11, 2015 for

Michael C. Wicks

This L^AT_EX 2 ε classfile conforms to the University of Notre Dame style guidelines as of Fall 2012. However it is still possible to generate a non-conformant document if the instructions in the class file documentation are not followed!

Be sure to refer to the published Graduate School guidelines at <http://graduateschool.nd.edu> as well. Those guidelines override everything mentioned about formatting in the documentation for this `NDDiss2 ε` class file.

It is YOUR responsibility to ensure that the Chapter titles and Table caption titles are put in CAPS LETTERS. This classfile does *NOT* do that!

*This page can be disabled by specifying the “noinfo” option to the class invocation.
(i.e.,\documentclass[... ,noinfo]{nddiss2e})*

This page is *NOT* part of the dissertation/thesis. It should be disabled before making final, formal submission, but should be included in the version submitted for format check.

`NDDiss2 ε` documentation can be found at these locations:

<http://www.gsu.nd.edu>
<http://graduateschool.nd.edu>

PLASMA FLOW CONTROL
FOR NOISE REDUCTION
ON A G550 NOSE LANDING GEAR: THE DEVELOPMENT OF A PLASMA
FAIRING

A Prospectus for a Dissertation

Submitted to the Graduate School
of the University of Notre Dame
in Partial Fulfillment of the Requirements

for the Degree of

Doctor of Philosophy

by

Michael C. Wicks

Flint O. Thomas, Director

Graduate Program in Aerospace and Mechanical Engineering

Notre Dame, Indiana

December 2015

© Copyright by
Michael C. Wicks
2015
All Rights Reserved

PLASMA FLOW CONTROL
FOR NOISE REDUCTION
ON A G550 NOSE LANDING GEAR: THE DEVELOPMENT OF A PLASMA
FAIRING

Abstract

by

Michael C. Wicks

Please note that the full \LaTeX source code (and an associated `Makefile`) is available from the University of Notre Dame Graduate Student Union web site. The Information Technology Committee page¹ has all the necessary files in download-able form. This particular dissertation was developed under Unix, but is also be usable under Windows with the appropriate \LaTeX setup and was modified on a Windows system in 2012-2013. It should also work with on Mac.

While the source code for this document provides an excellent example for how to use the `NDdiss2 ε` \LaTeX class to write a Notre Dame thesis, it is *not* a substitution for the documentation of the `NDdiss2 ε` \LaTeX class (also available on the ND GSU web site).

In this thesis, I will tell all that I know about Gnus. Gnus are wonderful little creatures that inhabit the center of the earth and give us wonderful and plentiful trees, dirt, and other earthly-things.

In short, we should love and cherish the Gnus. They can be very friendly, and are often mistaken for squirrels on the University of Notre Dame campus. Feed them

¹<http://www.gsu.nd.edu/>

whenever possible. If they get caught in trash cans, tip them over so that they can get out.

This abstract is going to continue on, including a few formulas, just for the sake of spilling over on to two pages so that we can see the author's name in the top right corner:

$$a^2 + b^2 = c^2$$

$$E = mc^2$$

$$\frac{e}{m} = c^2$$
$$a^2 + b^2 = \frac{e}{m}$$

These equations, by themselves mean nothing. But to the common Gnu, they define a whole way of living. While intricate mathematical implications certainly do not infiltrate the majority of humans' lives, every Gnu, from birth, is imbued with a sense of mathematical certainty and guidance. All Gnus, great and small, feel at one with mathematics. The cute furry bit is just a scam for their calculating minds.

To Laurimar

CONTENTS

FIGURES	v
TABLES	vi
CHAPTER 1: INTRODUCTION	1
1.1 Motivation	2
1.2 Theory of Aeroacoustics	3
1.3 Landing Gear	7
1.3.1 Geometry	7
1.3.2 Noise Sources	7
1.4 Literature Review	11
1.4.1 Single Cylinder Plasma Flow Control	12
1.4.2 Tandem Cylinders Plasma Flow Control	13
1.4.3 Shock Strut-Torque Arm Assembly Plasma Flow Control	14
CHAPTER 2: EXPERIMENTAL APPROACH	16
2.1 Experimental Objective	16
2.2 Experimental Facility	16
2.3 Notre Dame G550 Nose Landing Gear Model	16
2.4 Flow Visualization	18
2.5 Pressure Measurements	18
2.6 Microphone Measurements	18
2.7 Data Acquisition	18
2.8 Current Results	20
2.8.1 Wind Tunnel Background Noise Characterization	20
2.8.2 Far field check	20
2.8.3 Effects of Tripping	23
2.8.4 Comparison with University of Florida Anechoic Flow Facility Measurements	23
2.8.5 Baseline Sound Magnitude and Directivity	25
CHAPTER 3: OBJECTIVES AND FUTURE WORK	32
3.1 Research Objectives	32
3.2 Proposed Future Work	32
3.3 Conclusion	32

BIBLIOGRAPHY	33
------------------------	----

FIGURES

1.1	Photograph of Gulfstream 550 Nose Landing Gear.	8
1.2	Schematic view of Gulfstream 550 Nose Landing Gear components.	9
1.3	Flow Visualization of single cylinder in cross-flow with Spanwise and PSVG plasma actuators.	13
1.4	Flow Visualization of tandem cylinders in cross-flow with Spanwise and PSVG plasma actuators.	14
1.5	Flow Visualization of torque-arm assembly in cross-flow with Spanwise plasma actuators.	15
2.1	ND G550 model with and without plasma fairing installed.	17
2.2	Schematic of the polar array.	19
2.3	Photograph of the polar array installed in the ND AWT.	19
2.4	Representative far field noise level with and without Baseline 1 model installed at $\theta = 90^\circ$	21
2.5	Representative far field noise level with and without Baseline 1 model installed at $\theta = 90^\circ$	22
2.6	Comparison of far field noise level with and without the presence of a trip at $\theta = 90^\circ$	24
2.7	Comparison of far field noise level at UFAFF and ND AWT facilities at $\theta = 90^\circ$	26
2.8	Comparison of design of the NASA G550 and ND G550 model geometries.	26
2.9	1/3-octave band SPL	28
2.10	1/3-octave band SPL	29
2.11	Polar plot	30
2.12	Landing Gear Flow Visualization	31

TABLES

1.1	Physical mechanisms of flow-generated noise.	12
2.1	Data acquisition parameters.	20

CHAPTER 1

INTRODUCTION

Air travel in the U.S. is steadily growing due in part to an improving economy. Landings and take-offs at airports with FAA-operated towers and FAA-contracted towers are forecasted to increase from 48.9M to 59.9M or 22.5% between 2015 and 2035 [?]. With the continuing growth of air traffic, additional airports are being built and existing airports are expanding. As this occurs, it is hard to ignore a significant byproduct: the increase in aircraft noise.

The steady encroachment of airports is especially problematic in metropolitan areas, where aircraft noise can negatively impact quality of life. While this issue began as a public interest initiative, a recent study has found a statistically significant link between aircraft noise and cardiovascular disease [?]. Correia et al. looked at 89 of the largest airports across the U.S., and found that, even when controlling for other environmental factors, a 10 dB increase in noise was associated with a 3.5 % increase in hospital admissions in patients 65 years and older. Additional studies are ongoing, especially in the UK and EU, examining other potential adverse health effects such as delayed cognitive development in children, [?]. In light of these studies, it is clear: engineers and scientists have an ethical imperative to ensure the safety of technology.

Progress is being made in the field of aeroacoustics. In general, aircraft have become “quieter”, especially due to the widespread adoption of the turbofan jet engine. With the reduction of jet engine noise, aircraft noise has come to a level comparable to that of the airframe on approach and landing conditions [?]. The airframe is the new “lower noise barrier” of aircraft noise production. Efforts have

been taken to quantify airframe noise. Gibson performed flyover noise measurements and identified landing gears and high-lift devices as the two major noise contributors [?].

In addition to these efforts, several government initiatives have been launched to advance quiet aircraft technology. In the EU, European Visions 2020 requires to “reduce subjective noise impact by half” (minus 10 dB) per operation by 2020 relative to year 2000 level technology [?]. While in the US, the national Advanced Subsonic Transport (AST) and Quiet Aircraft Technology research programs have even more stringent milestones.

Due in part to these initiatives, many basic noise reduction technologies have been applied to aircraft landing gear.

Dobrzynski et al. studied the effect of solid, streamlined add-on fairings to various areas of main and nose landing gears. While these fairings were effective at reducing mid and high frequency noise levels, they also had adverse effects. This study and those like it revealed that solid fairings acted to increase local flow velocity and thereby noise from adjacent gear components.

The findings of solid fairing studies suggested that if flow could be Ravetta et al. Porous fairings

These technologies utilize passive flow control.

This study is focused on the application of active flow control.

1.1 Motivation

The present work is motivated to reduce noise produced by aircraft landing gear by flow control via application of DBD plasma actuators. To this end, experiments will be performed to 1) better understand the noise generation mechanisms present on aircraft landing gear, thereby aiding in the formation of flow control strategies. 2) Take steps toward the development of “plasma fairing” technology, which is a device

that can be retrofitted to existing aircraft landing gears with the purpose of reducing noise production.

In this chapter, the physics of airframe noise production are discussed. The structure of Aircraft landing gear is presented. This geometry is grouped into two main sub-systems and flow control strategies are recommended for both. Areas of noise contribution are considered and the underlying physical mechanisms are identified. Finally, the literature is reviewed with respect to the application of Plasma Flow Control to increasingly complex geometries.

1.2 Theory of Aeroacoustics

To arrive at a viable flow control strategy, it is useful to first review the underlying physics. The modern theory of aeroacoustics, that is sound generated by aerodynamic means, is based on James Lighthill's so-called acoustic analogy. He states that sound generated in a fluid flow is only important in regions of turbulent fluctuations [1]. Based on this assumption, the Navier-Stokes Equation and isentropic equation of state in indicial notation are

$$\frac{\partial \rho}{\partial t} + \frac{\partial(\rho u_i)}{\partial x_i} = 0, \quad (1.1)$$

$$\frac{\partial(\rho u_i)}{\partial t} + \frac{\partial(\rho u_i u_j + P_{ij})}{\partial x_j} = 0, \quad (1.2)$$

$$c_o^2 = \frac{\partial p}{\partial \rho}|_{s=const.} = \frac{p'}{\rho'} \quad (1.3)$$

where

$$P_{ij} = p' \delta_{ij} - \sigma_{ij}. \quad (1.4)$$

P_{ij} is the total stress tensor including pressure and viscous terms, ρ is the fluid density, u is the local velocity vector, p is the pressure and c_o is the local speed of sound. Also, $p' = p - p_o$ and $\rho' = \rho - \rho_o$ represent the fluctuating pressure and density relative to the mean values, respectively. After assuming sufficiently small fluctuations, equations 1.1 and 1.2 can be linearized yielding the classical Lighthill's equation

$$\frac{\partial^2 \rho}{\partial t^2} - c_o^2 \nabla^2 \rho = \frac{\partial^2 T_{ij}}{\partial x_i \partial x_j}, \quad (1.5)$$

where the source term T_{ij} is known as Lighthill's turbulence stress tensor

$$T_{ij} = \rho u_i u_j + P_{ij} - c_o^2 (\rho - \rho_0) \delta_{ij}, \quad (1.6)$$

and where δ_{ij} is the Kronecker delta which is defined as,

$$\delta_{ij} = \begin{cases} 1 & \text{if } i = j \\ 0 & \text{if } i \neq j \end{cases}. \quad (1.7)$$

For the special case of high Reynolds number, incompressible flow, both the density fluctuations and the viscous stresses are negligible, reducing the Lighthill stress tensor to

$$T_{ij} \approx \rho_0 u_i u_j. \quad (1.8)$$

Equation 1.5 can be solved and formulated in terms of p' by combining with equation 1.3 giving

$$p' = c_o^2 \rho' = \frac{1}{4\pi} \frac{\partial^2}{\partial x_i \partial x_j} \int_V \frac{T_{ij}}{r} dV, \quad (1.9)$$

where V represents the volume of the region of interest, and r represents the

distance to the acoustic source.

In 1955, Lighthill's analogy was extended to account for the presence of solid boundaries within the turbulent flow region [?]. The general solution to this equation is

$$p' = \underbrace{\frac{1}{4\pi} \frac{\partial^2}{\partial x_i \partial x_j} \int_V \left[\frac{T_{ij}}{r} \right] dV}_{I} - \underbrace{\frac{1}{4\pi} \frac{\partial}{\partial x_j} \int_S \left[\frac{P_{ij} + \rho u_i u_j}{r} \right] n_i dS}_{II} + \underbrace{\frac{1}{4\pi} \frac{\partial}{\partial t} \int_S \left[\frac{\rho u_i}{r} \right] n_i dS}_{III}, \quad (1.10)$$

where S represents the control surface bounding the volumetric region of interest [?]. Equation 1.10 forms the basis of airframe noise generation by including the effects of reflection and diffraction of acoustic waves at the boundaries.

To illustrate the nature of the acoustic source terms on the right hand side of equation 1.10, an order-of-magnitude scaling analysis is performed with the purpose of determining the radiation patterns of the hypothetical acoustic source with respect to flow speed, U_o , and propagation distance, r . Lighthill conveniently used a subsonic, turbulent isothermal jet to define a physical application for which characteristic length, frequency, pressure scales, and velocity are defined [?]. Substituting the pertinent characteristic scales yields the following order-of-magnitude approximations for the components of the acoustic source term:

$$\int_V dV \propto D^3 \quad (1.11)$$

$$T_{ij} \propto \rho_o U_o^2 \quad (1.12)$$

$$\frac{\partial}{\partial x_i} = \frac{\partial}{c_o \partial t} \propto \frac{f}{c_o} \propto \frac{U_o}{c_o D} \quad (1.13)$$

Equations 1.11 - 1.13 are then utilized to replace the source terms in equation 1.10, resulting in the following:

$$I : \frac{1}{4\pi} \frac{\partial^2}{\partial x_i \partial x_j} \int_V \left[\frac{T_{ij}}{r} \right] dV \propto \left(\frac{U_o}{c_o D} \right)^2 (D^3) \left(\frac{\rho_o U_o^2}{r} \right) \propto \frac{U_o^4}{r}, \quad (1.14)$$

$$II : \frac{1}{4\pi} \frac{\partial}{\partial x_j} \int_S \left[\frac{P_{ij} + \rho u_i u_j}{r} \right] n_i dS \propto \left(\frac{U_o}{c_o D} \right) \left(\frac{\rho_o U_o^2}{r} \right) (D^2) \propto \frac{U_o^3}{r}, \quad (1.15)$$

$$III : \frac{1}{4\pi} \frac{\partial}{\partial t} \int_S \left[\frac{\rho u_i}{r} \right] n_i dS \propto \left(\frac{U_o}{D} \right) \left(\frac{\rho_o U_o}{r} \right) (D^2) \propto \frac{U_o^2}{r}. \quad (1.16)$$

This analysis assumes that the freestream Mach number is much less than unity or $M = \frac{U_o}{c_o} \ll 1$, and that far-field acoustic radiation dominates the signal so that it acts as a spherically-spreading pressure wave.

Furthermore, the radiated acoustic power W , is proportional to the square of the pressure field, giving

$$I : W \propto p'^2 \propto \frac{U_o^8}{r^2}, \quad (1.17)$$

$$II : W \propto p'^2 \propto \frac{U_o^6}{r^2}, \quad (1.18)$$

$$III : W \propto p'^2 \propto \frac{U_o^4}{r^2}. \quad (1.19)$$

The results of the scaling analysis presented in equation 1.17 correspond physically to the radiation pattern of a volumetric distribution of quadrupole sources. Therefore, Lighthill's acoustic analogy states that the far-field acoustic pressure field of a region of turbulence in a steady flow, and a region of quadrupole acoustic sources with

no flow are equivalent. Similarly, equations 1.18 and 1.19 represent a distribution of dipole and monopole sources, respectively. Finally, this analysis shows that a decrease in acoustic power of the system corresponds to an increase in acoustic efficiency when transitioning from a quadrupole to a dipole to a monopole. These trends are extremely useful in determining the nature of the acoustic sources present in flows around complex geometries, such as around aircraft landing gears.

1.3 Landing Gear

As previously stated, aircraft landing gear have been identified as a primary source of airframe noise especially for the larger wide-body configurations [1].

Landing gear generally come in two types: nose landing gear (NLG) and main landing gear (MLG). The former is designed for steering while the latter is designed for braking.

The scope of this study is limited to work on the G550 nose landing gear, but while many designs vary in each aircraft, it is probable that flow control strategies will overlap.

1.3.1 Geometry

The Gulfstream G550 Nose landing gear was selected due to an industry collaboration with NASA. In Neuhart et al., this design was aerodynamically characterized to provide a database of aerodynamic and acoustic data by which to compare experiments and simulations.

The actual landing gear is depicted in Figure 1.1 for reference, and shown schematically in Figure 1.2.



Figure 1.1. Photograph of Gulfstream 550 Nose Landing Gear.

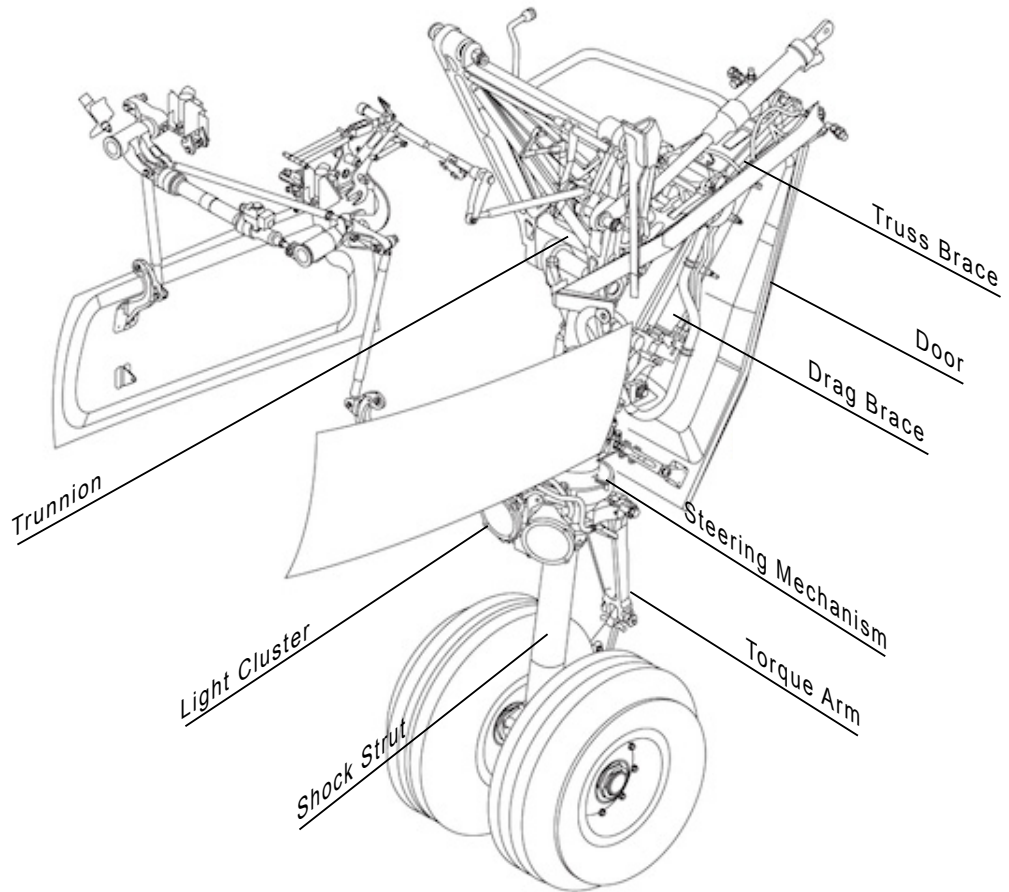


Figure 1.2. Schematic view of Gulfstream 550 Nose Landing Gear components.

1.3.2 Noise Sources

Recall that adding a solid boundary to the flow drastically altered the source terms in equation 1.10. In experiments, these terms manifest as flow-generated noise. Typically there are two types:

- Tonal - generated by periodic flow events (such as vortex shedding),
- Broadband - generated by random flow events (such as turbulence).

Most aerodynamic bodies are characterized by their drag force. When a body is streamlined, it is said that the total drag is dominated by the viscous drag component. However, for some bodies the total drag is dominated by the pressure drag component, these bodies are referred to as bluff. Bluff bodies can be a major contributor to flow-generated noise, due in part to the unsteady wake these structures tend to cause. The canonical example of a bluff body is a simple cylinder, for which the flow is well understood. It is dominated by large-scale von Karman vortex shedding of frequency f , over the cylinder body of characteristic length L . This vortex shedding frequency is characterized by the dimensionless Strouhal number $St = \frac{fL}{U_\infty}$, which is constant over a wide range of Reynolds numbers $Re = \frac{\rho U_\infty L}{\mu}$ [?], where ρ and μ represent mean density and dynamic viscosity of the freestream flow, respectively. This large-scale vortex shedding corresponds to periodic unsteady surface pressure which is responsible for the generation of tonal noise.

More complex geometries such as the landing gear, can be considered as a collections of bluff bodies. Counter-intuitively, the acoustic signature for the landing gear is broadband in nature which is associated with turbulence [?]. As depicted in Figure 1.1, the landing gear components are arranged in close proximity to one another. It is possible that this proximity stifles full wake development, effectively preventing the large-scale vortex shedding observed for the simple cylinder. This suggests that flow control on fundamental geometries, while useful, may not be representative of

the actual flow physics. This is the foundation for the previously suggested strategy of examining sub-systems.

In addition to varying inter-component spacings, the presence of multiple length scales in the landing gear geometry implies that some components may also contribute to the total noise as reflective sources. Guo et al. divided the far-field noise propagation into three regimes based on the concept of acoustic compactness [?]. Since an acoustic wave in a medium is governed by the speed of sound then $c_o = \lambda f$. A source is said to be acoustically compact if $kL \ll 1$ where k is the acoustic wavenumber defined as $k = \frac{2\pi}{\lambda} = \frac{2\pi f}{c_o}$, λ is the acoustic wavelength, and L is the characteristic length. It is noncompact if $kL \geq 1$. For a full-scale Boeing 737 main landing gear large (wheels and doors) and medium geometries (main struts and linkages) represented low and mid-range frequencies, respectively. Small geometries (hoses, sharp edges, and electrical wiring) represented high frequency noncompact acoustic sources. While compact sources behave like a distribution of dipoles, noncompact sources represent phase variations in surface pressure leading to degradation of radiation efficiency (quadrupole).

Before discussing a strategy for flow control, it is useful to first consider the physical phenomena present. While quantifying the contribution of each mechanism to the total acoustic signature of the landing gear, is a fairly difficult task, an order-of-magnitude analysis can be applied to estimate a potential dominant source. Table 1.1 lists the sources considered, corresponding acoustic power, noise type, and source type. Recall that high acoustic power corresponds to low acoustic efficiency, meaning a monopole source is a more effective noise producer than a quadrupole source. Focusing on the more efficient dipole sources present, the mechanisms of unsteady wake and downstream wake impingement are the most viable candidates for flow control. Vortex shedding may be present but is highly tonal, and the broadband nature of landing gear noise suggests that this is probably a minor noise producer.

TABLE 1.1
Physical mechanisms of flow-generated noise.

Mechanism	Acoustic Power	Source Type	Noise Type
Vortex Shedding	$\frac{U_o^6}{r^2}$	Dipole	Tonal
Wake Shear Layer	$\frac{U_o^8}{r^2}$	Quadrupole	Broadband
Wake Turbulence	$\frac{U_o^8}{r^2}$	Quadrupole	Broadband
Downstream Wake Impingement	$\frac{U_o^6}{r^2}$	Dipole	Broadband
Unsteady Wake	$\frac{U_o^6}{r^2}$	Dipole	Broadband
Reflective Sources	$\frac{U_o^8}{r^2}$	Quadrupole	Tonal or Broadband

These physical phenomena are considered in the following review of literature.

1.4 Literature Review

This section provides a review of aeroacoustic research pertinent to the development of a plasma fairing

1.4.1 Single Cylinder Plasma Flow Control

The single cylinder is the most simplified representation of the landing gear strut. Active flow control efforts by means of DBD plasma actuators were first applied to this generic bluff body geometry as proof-of-concept. Several experiments and large-eddy simulations (LES) were performed at the University of Notre Dame to show the viability of this technology [?]. Two flow control strategies were employed: spanwise plasma actuators, and plasma streamwise vortex generators (PSVGs). The latter of these devices is made up of a spanwise array of electrodes oriented in the streamwise direction. Flow visualization of these techniques is shown in Figure 2.12.

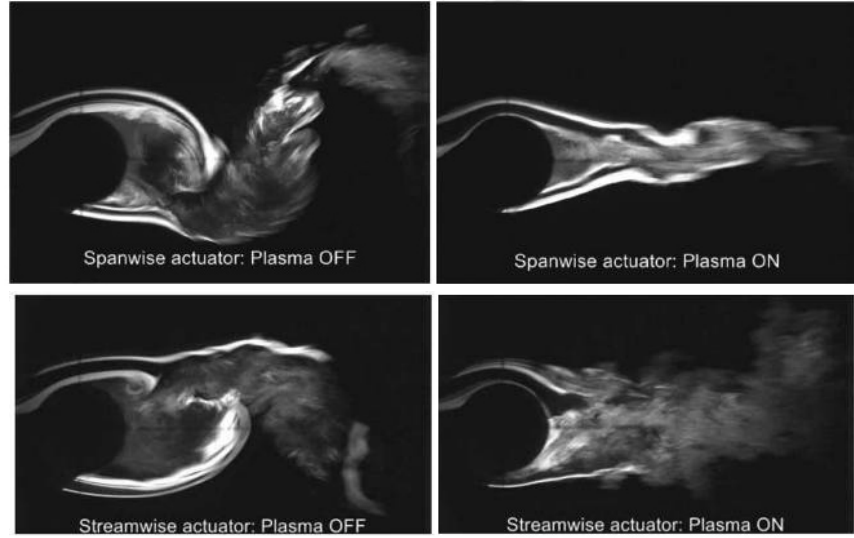


Figure 1.3. Flow Visualization of single cylinder in cross-flow with Spanwise and PSVG plasma actuators.

Both approaches were effective in significantly suppressing Karman vortex shedding, if by different mechanisms. Spanwise plasma actuators achieve flow control through modification of the detached free shear layer. PSVGs induce streamwise voricity into the nascent cylinder wake, promoting rapid wake mixing. Kozlov et al. performed near field microphone measurements with $d = 0.61$ m, demonstrating a reduction in noise levels of 11.2 dB and 14.2 dB for spanwise actuators and PSVGs, respectively. These results were promising and inspired more studies on a slightly more complex geometry: tandem cylinders.

1.4.2 Tandem Cylinders Plasma Flow Control

The tandem cylinders configuration is the next stage in the development of flow control for aircraft landing gear. The interaction between the two bluff bodies represents that between main strut and downstream components.

Zdravkovich comprehensively reviewed two circular cylinders of the same diameter at subcritical Reynolds number.

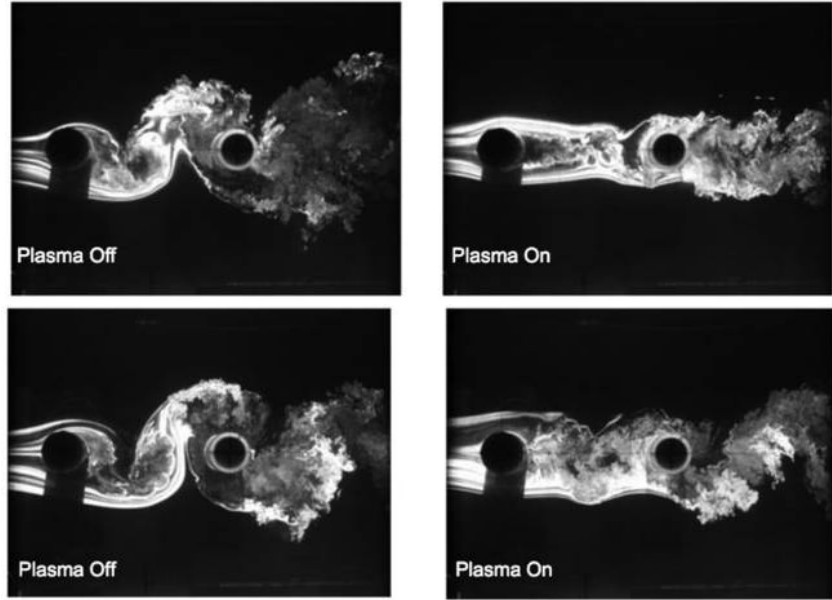


Figure 1.4. Flow Visualization of tandem cylinders in cross-flow with Spanwise and PSVG plasma actuators.

[?]

[?] [?] [?]

1.4.3 Shock Strut-Torque Arm Assembly Plasma Flow Control

Huang et al. studied the acoustic of plasma actuators on a torque arm apparatus. By applying spanwise plasma actuators in both an 'upstream' and 'downstream' configuration, two types of flow control were explored. The upstream configuration served to create a virtual plasma fairing effect by routing the shear layers around the downstream components, reducing the overall noise generated by wake impingement. The downstream configuration is shown to have reduced vortical structures, lowering the unsteadiness in the wake. [?] [?]

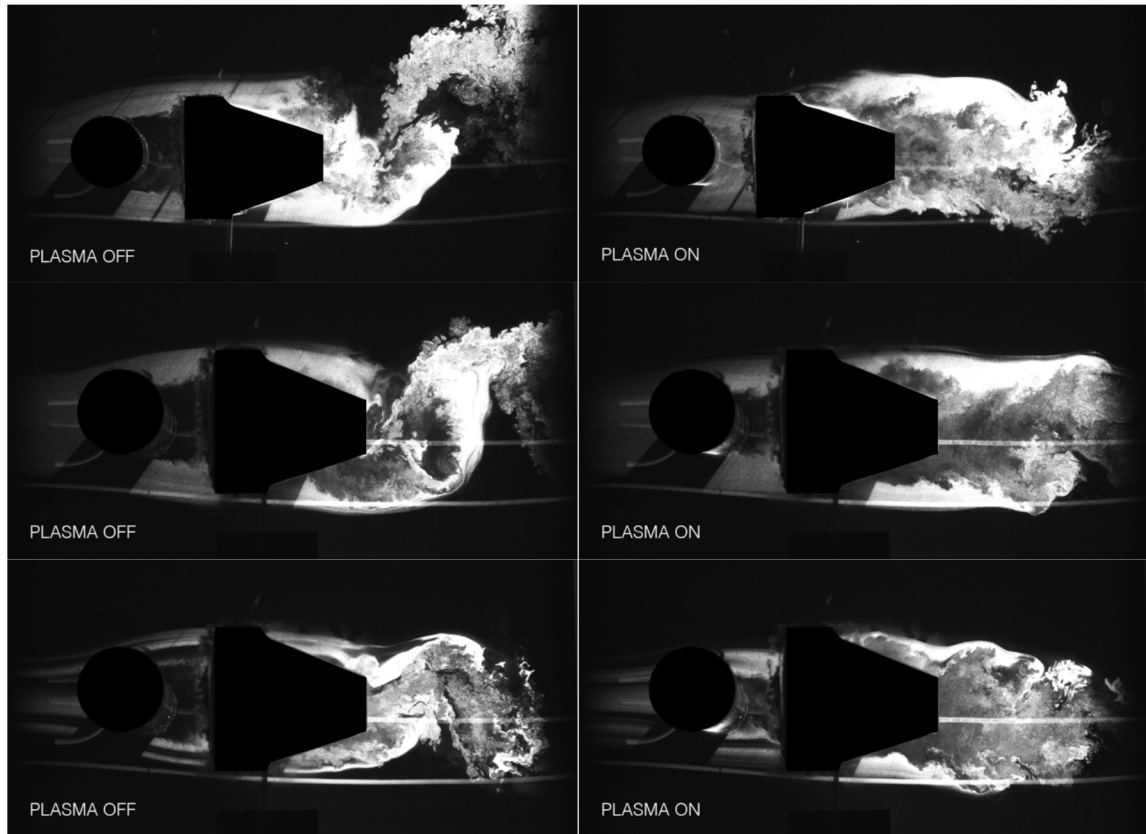


Figure 1.5. Flow Visualization of torque-arm assembly in cross-flow with Spanwise plasma actuators.

CHAPTER 2

EXPERIMENTAL APPROACH

2.1 Experimental Objective

2.2 Experimental Facility

Baseline acoustic measurements without plasma flow control were obtained in the Notre Dame Anechoic Wind Tunnel Facility (ND AWT). The ND AWT is a low-noise, open-jet acoustic wind tunnel with a free jet test section measuring 24-in-(0.610 m)-high by 24-in-(0.610 m)-wide installed in a large anechoic chamber suitable for frequencies above 100 Hz. The maximum empty test section velocity is approximately $U_\infty = 35$ m/s. The maximum safe tunnel velocity with the Notre Dame G550 Nose Landing Gear 30%-scale model (ND G550) installed is 30 m/s corresponding to a Mach number of $M_\infty = 0.1$.

Atmospheric properties such as ambient temperature and pressure were acquired using a digital thermometer and barometer. The tunnel speed is measured using a pitot-static probe installed approximately 6 in (0.154 m) from the free jet inlet centerline. From these data local sonic speed and the flow Mach number is computed.

2.3 Notre Dame G550 Nose Landing Gear Model

Acoustic measurement for two baseline landing gear model configurations were performed. The first, designated Baseline 1, consisted of the ND G550 model without the plasma fairing installed, which is shown in the photograph of Figure 2.1a. The second, designated Baseline 2, involved the ND G550 model retrofitted with a plasma



(a) Baseline 1



(b) Baseline 2

Figure 2.1. ND G550 model with and without plasma fairing installed.

fairing assembly in order to facilitate installation of dielectric barrier discharge (DBD) plasma actuators for flow control. This configuration is shown in the photograph of Figure 2.1b. None of the acoustic measurements presented in this report for both configurations involved the use of plasma flow control. Rather, the focus was on the characterization of baseline acoustics for both configurations.

2.4 Flow Visualization

2.5 Pressure Measurements

2.6 Microphone Measurements

A polar array of omnidirectional microphones was used to acquire far field noise level spectra along the length of the AWT test section. It consists of a 1/2-in ACO Model 7046 electret microphone with companion 4012 preamplifier and PS9200 power supply. A schematic illustrating the array is shown in Figure 2.2. Additionally, the array configuration relative to the G550 model is shown in the photograph of Figure 2.3. The microphone is mounted using a microphone stand so as to protrude from an acoustically treated rail by approximately 13 in (0.330 m). The total range of acoustic source-to-microphone angle spanned by the polar array is approximately $30^\circ \leq \theta \leq 150^\circ$ as referenced from the upper torque arm of the model in the downstream flow direction. As shown in Figure 2.3, the polar array is situated along the length of the free jet test section and positioned at the same height as the upper torque arm of the model, with the plane of the microphone located approximately 59 in (1.50 m) from the test section centerline.

2.7 Data Acquisition

For microphone data acquisition, a National Instruments USB-6343 DAQ was used, yielding a total of 45 available channels with 48-bit ADC. The sampling pa-

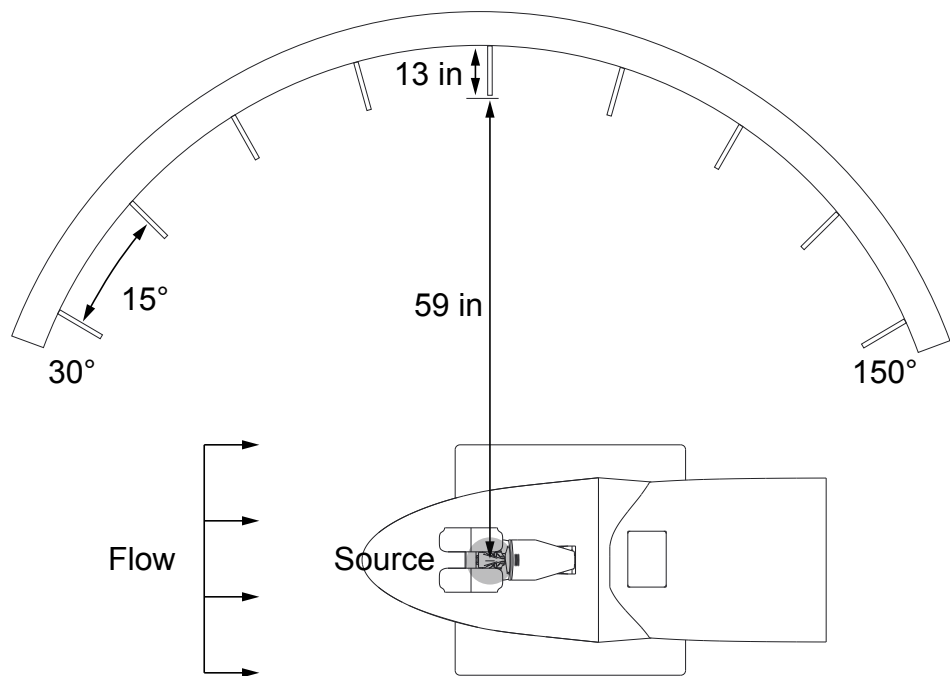


Figure 2.2. Schematic of the polar array.

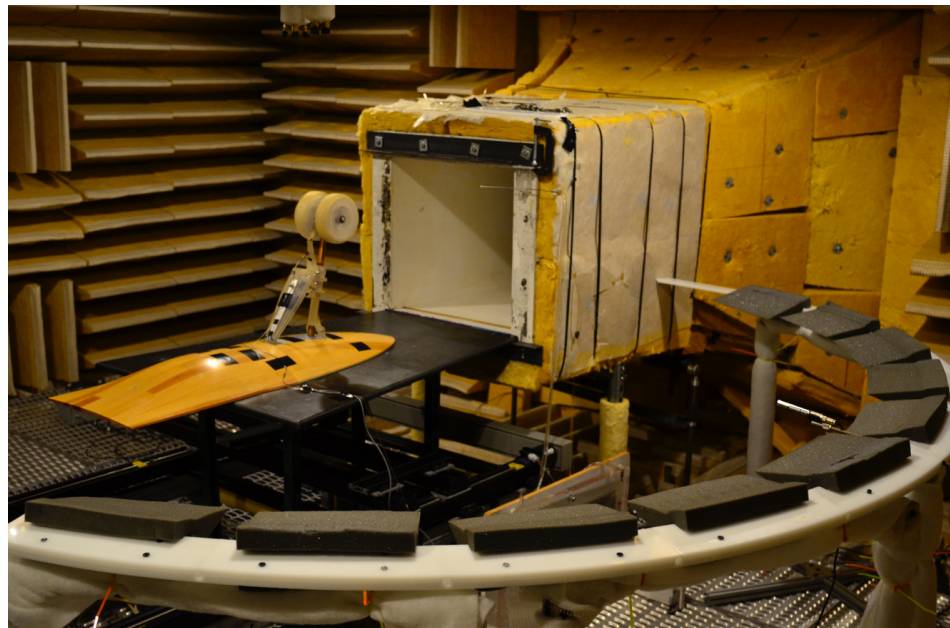


Figure 2.3. Photograph of the polar array installed in the ND AWT.

TABLE 2.1

Data acquisition parameters.

Sensors	Sampling Rate (Hz)	$\frac{Samples}{block}$	Window Function	Overlap (%)	N_{blocks}	$N_{averages}$	Acquisition Time (s)
ACO	65,536	2048	Hanning	0	960	960	30

rameters for the microphone data acquisition are listed in Table 2.1.

2.8 Current Results

2.8.1 Wind Tunnel Background Noise Characterization

It was deemed important to establish that the background noise levels in the ND AWT were sufficiently below that of the ND G550 model. To that end, measurement of noise levels for both Baseline 1 and Baseline 2 G550 configurations were compared with those obtained with the AWT tunnel running empty. Figure 2.4 presents a representative comparison of 1/3-octave band sound pressure level (SPL) spectra obtained for the Baseline 1 configurations and the empty tunnel. The figure clearly shows that the background empty tunnel noise level is several orders of magnitude below that of the ND G550, so that the effects of plasma flow control on noise production will be detectable in this facility.

2.8.2 Far field check

This section describes a procedure for verifying the far field assumption for microphone measurements.

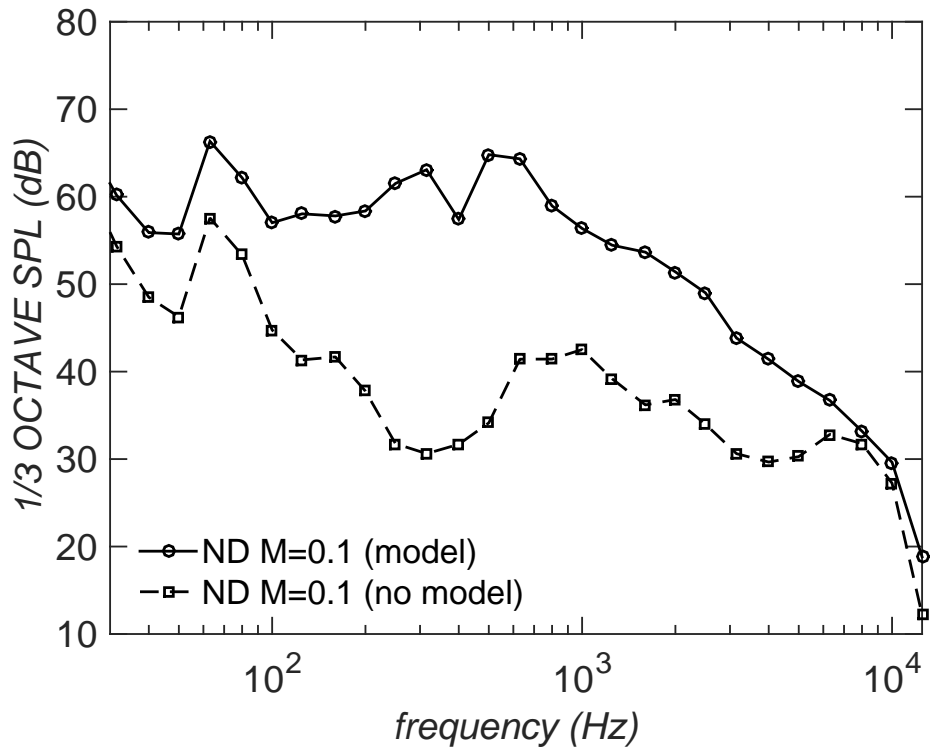


Figure 2.4. Representative far field noise level with and without Baseline 1 model installed at $\theta = 90^\circ$

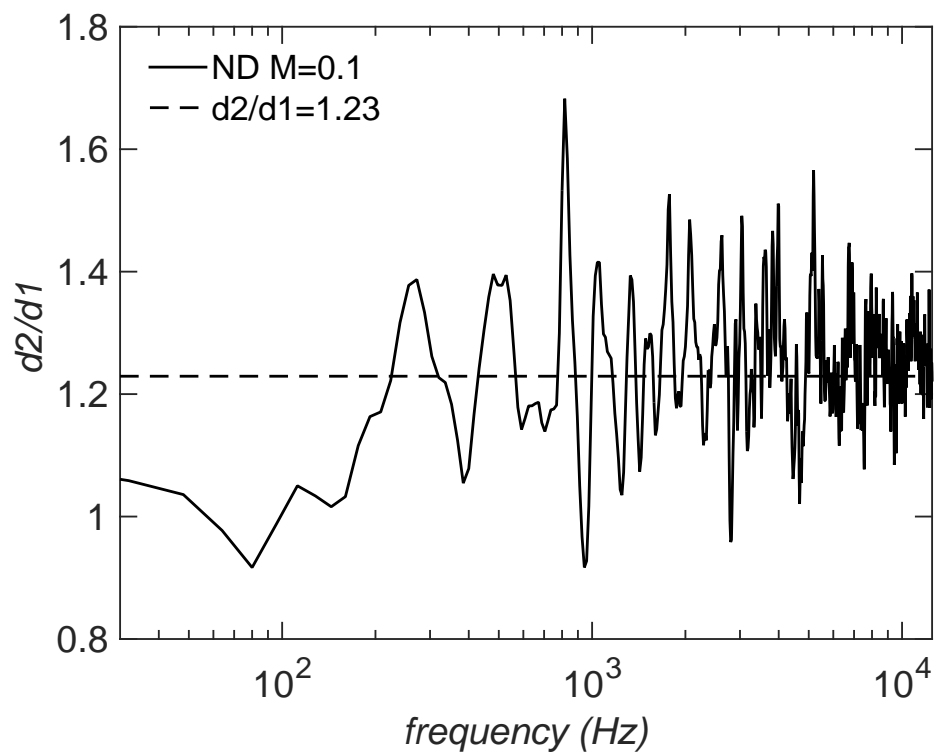


Figure 2.5. Representative far field noise level with and without Baseline 1 model installed at $\theta = 90^\circ$

2.8.3 Effects of Tripping

Previous work on the NASA G550 Nose Landing Gear (NASA G550) involved application of serrated transition strips that were applied along the length of the shock strut in order to create a turbulent boundary layer prior to separation. For consistency with this previous work, the influence of similar aerodynamic trips was explored on the ND G550 Baseline 1 model. A distributed roughness element made of standard diving board tape was fixed to the shock strut. Sample results comparing 1/3-octave band SPL spectra for the tripped and untripped cases are presented in Figure 2.6. This figure shows that there was very little influence of the trip on radiated noise. Since a trip would restrict the optimum placement of the plasma actuators, it was omitted from the model and the acoustic results that follow were obtained without tripping unless otherwise indicated.

2.8.4 Comparison with University of Florida Anechoic Flow Facility Measurements

To match the numerical simulations being performed concurrently in this study, the far field microphone distance d , was 72 in (1.83 m) array-to-model and 59 in (1.50 m) microphone-to-model. However, previous studies conducted at the University of Florida Anechoic Flow Facility (UFAFF) on the NASA G550 model were performed at a source-to-microphone distance of 48 in. In order to form a basis for comparison with acoustic results from that study, 1/3-octave band SPL spectra were obtained with the ND Baseline 1 model in the ND AWT for a source-to-microphone distance of 48 in (1.22 m). Even after accounting for the source-to-microphone distance disparity, the UFAFF experiments were performed at a freestream Mach number $M_\infty = 0.189$ and the Notre Dame experiments were performed at $M_\infty = 0.1$. The effect of disparate Mach numbers on the SPL can be accounted for by scaling the Notre Dame results via the relation,

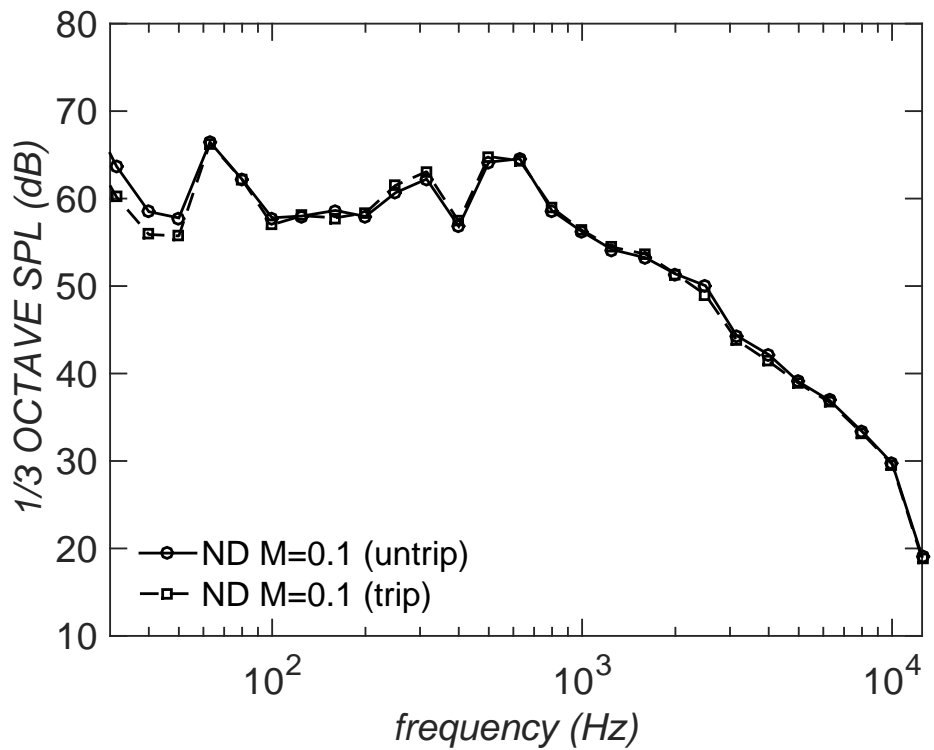


Figure 2.6. Comparison of far field noise level with and without the presence of a trip at $\theta = 90^\circ$

$$SPL_2 = SPL_1 - 10 \log \left(\frac{M_1}{M_2} \right)^6, \quad (2.1)$$

where SPL_1 and M_1 denote the ND AWT experimental values, M_2 denotes the UFAFF test Mach number (0.189) and SPL_2 represents the ND AWT sound pressure level values corrected for Mach number. Figure 2.7 compares 1/3-octave band SPL spectra obtained in both facilities for the case of $\theta = 90^\circ$. In this plot the frequency is expressed in terms of Strouhal number, $St_D = fD/U_\infty$, where length scale D is the shock strut diameter upstream of the torque arm and U_∞ is the freestream velocity. There is good collapse of the NASA G550 and ND G550 data from $0.3 \leq St_D \leq 0.6$. Below this range there is about 4-5 dB difference before the 100 Hz AWT cutoff frequency. Above this range there is significant discrepancy. The NASA G550 model is characterized by a peak near $St_D = 3$ and spectral roll-off above this peak. The ND G550 model lacks this high frequency content. The components of the ND G550 model are mostly fabricated from SLA plastic, while the NASA G550 consists of mostly aluminum and carbon fiber. To compensate for the differences in tensile strength, thickness was added to several components of the ND G550 model as shown in the CAD images in Figure 2.8. Additionally, it was necessary to construct most of the ND G550 model from plastic to facilitate the retrofitting of plasma actuators. It is possible, but by no means certain that these design modifications may play a role in the observed differences in noise spectra.

2.8.5 Baseline Sound Magnitude and Directivity

The Overall Sound Pressure Level (OASPL) is calculated by integrating the power spectral density from $100 \leq f \leq 12,500$ Hz. OASPL at each location of the polar array, $30^\circ \leq \theta \leq 150^\circ$, is given in Figure 2.11. Baseline far field 1/3-octave band spectra are reported for each location on the polar array in Figure 2.9. There is

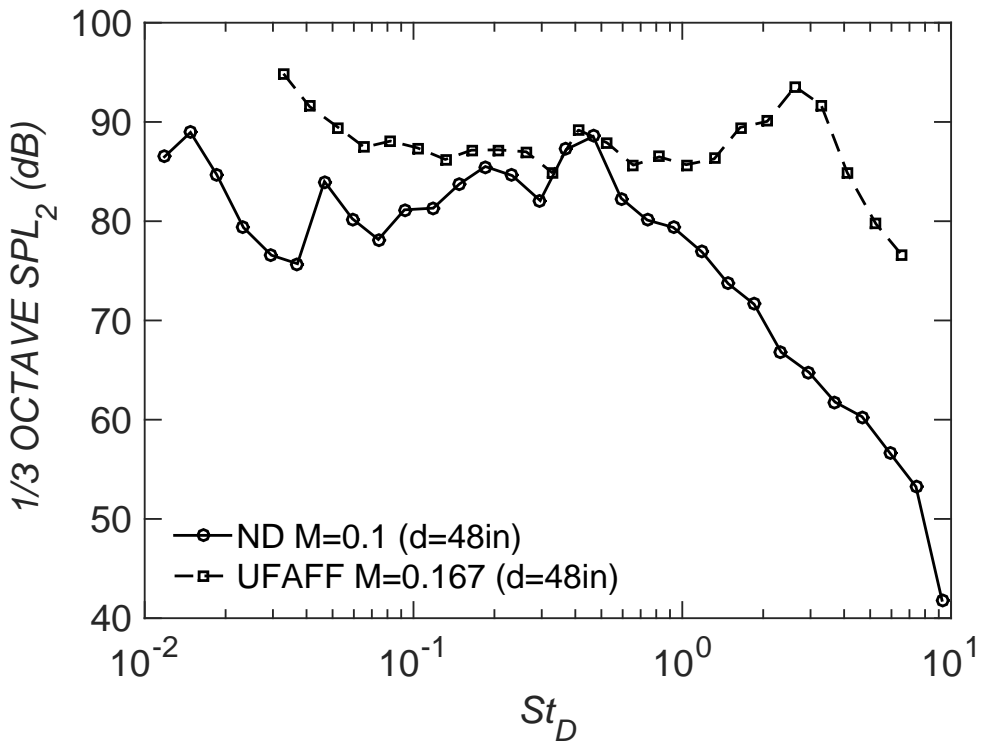


Figure 2.7. Comparison of far field noise level at UFAFF and ND AWT facilities at $\theta = 90^\circ$

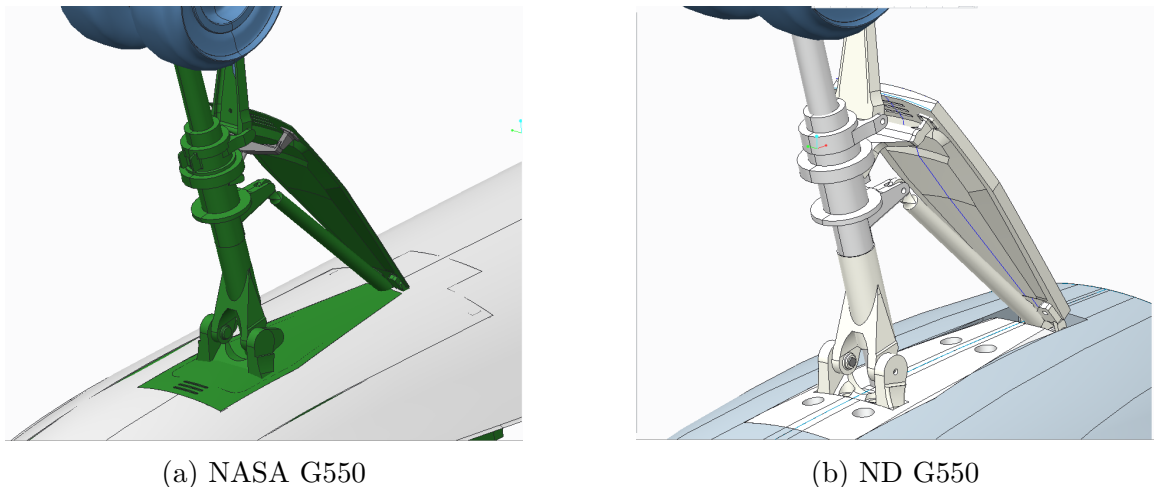
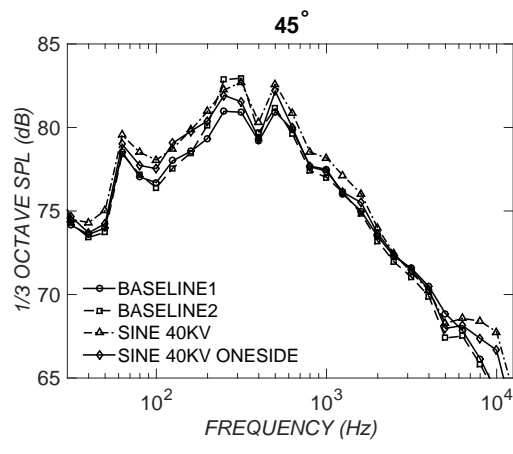
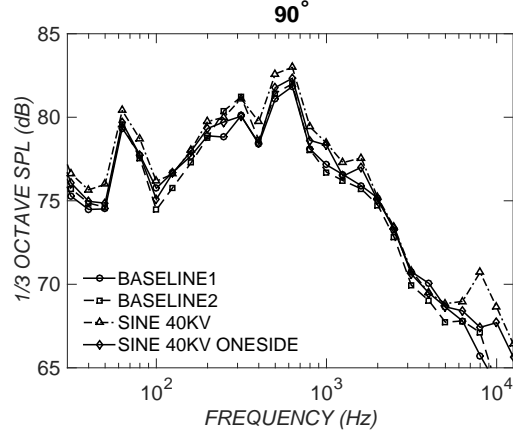


Figure 2.8. Comparison of design of the NASA G550 and ND G550 model geometries.

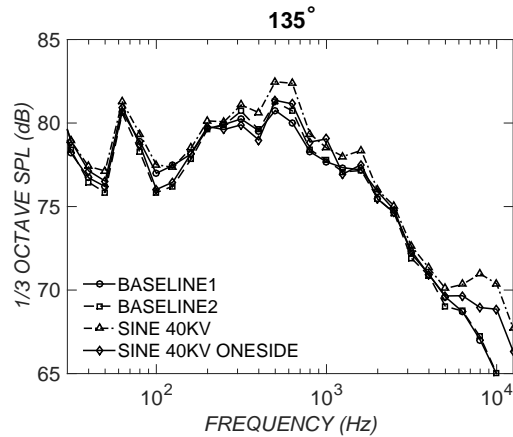
consistent noise reduction of about 6 dB observed at each microphone location from $100 \leq f \leq 200$ Hz. Additionally, the twin peaks at 300 Hz and 500 Hz respectively show up as one peak at 300 Hz for the $\theta = 30^\circ$ location. These spectral peaks increase in magnitude with increasing θ , for $\theta \leq 90^\circ$, and decrease in magnitude for $90^\circ < \theta \leq 150^\circ$. Similar observations were made in unsteady pressure during the Phase I study on the ND torque arm model, suggesting that these peaks are characteristic of the torque arm section of the ND G550 model. However, this will need to be substantiated with unsteady pressure data on the ND G550, which will be included in the next report. Finally, the shape of the partial directivity plot exhibits dipole-like behavior.



(a) $\theta = 45^\circ$



(b) $\theta = 90^\circ$



(c) $\theta = 135^\circ$

Figure 2.9. 1/3-octave band SPL

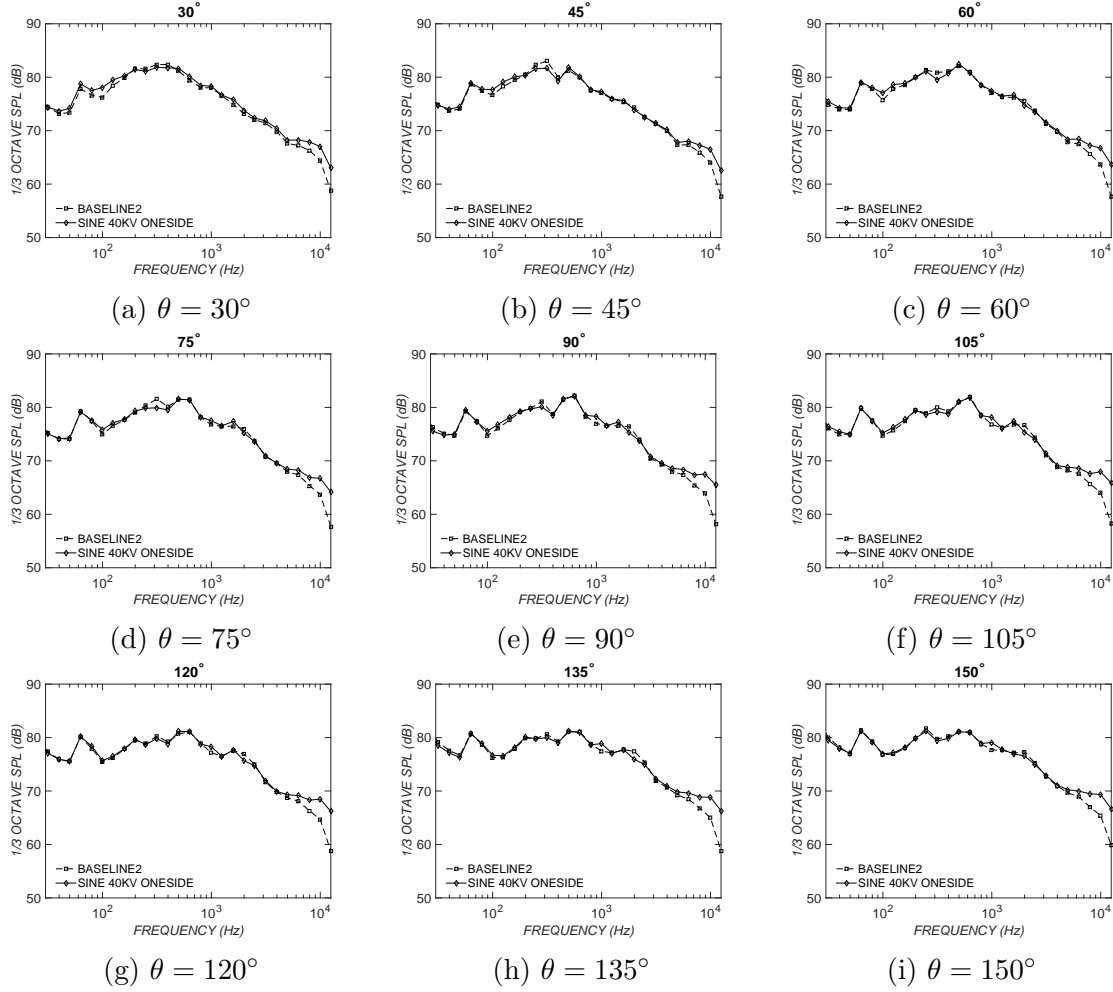


Figure 2.10. 1/3-octave band SPL

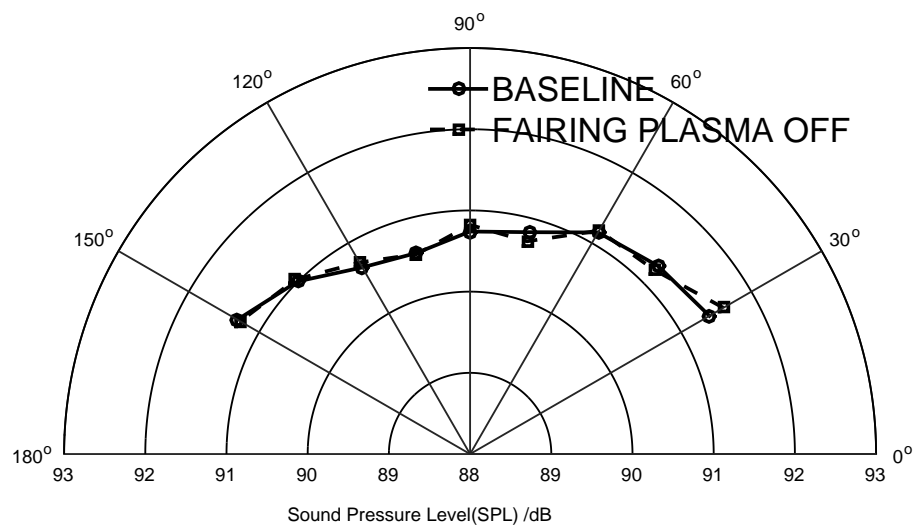




Figure 2.12. Landing Gear Flow Visualization

CHAPTER 3

OBJECTIVES AND FUTURE WORK

3.1 Research Objectives

3.2 Proposed Future Work

3.3 Conclusion

BIBLIOGRAPHY

1. M. S. Howe. *Theory of Vortex Sound - Lighthill's Theory*. Cambridge University Press, 2003.

This document was prepared & typeset with pdfL^AT_EX, and formatted with NDDiss2_ε classfile (v3.2013[2013/04/16]) provided by Sameer Vijay and updated by Megan Patnott.